Performance Characteristics of a Coaxial Pulsed Plasma Thruster with Teflon Cavity

Toshiaki Edamitsu, Hirokazu Tahara and Takao Yoshikawa
Department of Mechanical Science and Bioengineering,
Graduate School of Engineering Science, Osaka University
1-3 Machikaneyama, Toyonaka, Osaka 560-8531, JAPAN
Phone: +81-6-6850-6179, Fax: +81-6-6850-6179
E-mail: edamitsu@yoshikawa.me.es.osaka-u.ac.jp

Abstract

A coaxial pulsed plasma thruster (PPT) with a Teflon cavity was designed, and its performance characteristics were examined varying stored energy, cavity length and capacitance. The PPT was tested as the entire system including the discharge circuit, and the results were explained with both the transfer efficiency and the acceleration efficiency. The transfer efficiency is defined as the fraction of energy in capacitors supplied into plasma, and the acceleration efficiency as the fraction of energy supplied into plasma converted to thrust energy. To estimate these efficiencies, the equivalent plasma resistance was defined and calculated using energy conservation during discharge. The equivalent plasma resistance proportionally increased with cavity length, and therefore the current peak increased with decreasing cavity length. The energy density calculated by the transfer efficiency was increased with decreasing cavity length. As a result, higher acceleration efficiency and lower transfer efficiency were obtained with shorter cavity length. Accordingly, there was an optimal cavity length for the thrust efficiency. The specific impulse and the impulse bit per unit stored energy ranged from 390 s and 50 μ Ns/J for a cavity length of 34 mm to 825 s and 11 μ Ns/J for a cavity length of 4 mm when the stored energy was fixed to 21.4J. Thus, it was showed that the performance of this PPT approached that of electromagnetic-acceleration-type PPT with decreasing cavity length. The PPT achieved thrust efficiencies of 10-12% at 21.4 J and 6-7% at 5.35 J at cavity lengths between 14 mm and 29 mm.

Introduction

A lot of studies about pulsed plasma thruster (PPT) have been carried out because the PPT has some features superior to other kinds of electric propulsion. The PPT has no sealing parts, simple structure, high reliability, which are benefits of using solid propellant. The electromagnetic-acceleration -type PPT generally has higher specific impulse but lower thrust efficiency than electrothermal -acceleration-type PPTs. However, performances of both PPTs are rather low as compared with other electric thrusters.

In present study, a PPT with a cavity of propellant is designed in order to investigate the cause of low performances and to improve them. This PPT mainly accelerates propellant by high pressure generated by the high-current discharge in the cavity. The cavity diameter is 3mm, which is smaller than that of conventional electrothermal PPTs with relatively high pressure in the cavity[1),2)]. In addition, the electromagnetic acceleration may be expected by the divergent current in the cathode nozzle.

Various energy efficiencies were defined in Ref. 3). In this study, the thrust efficiency, the transfer efficiency and the acceleration efficiency are investigated in detail. It is important to know performances of the discharge circuit and the thruster head, and the relationship between them, in order to improve the performance as a whole system.

In order to investigate these efficiencies, a lot of measurements were carried out. Main objects of this study are, (1) to evaluate the performance of designed PPT, especially the effect of cavity length and energy on the PPT, (2) to investigate the relationship between the discharge circuit and the PPT performance, and (3) to fit curves to the results in order to understand the PPT's performance simply.

Experimental Apparatus and Procedure

The experimental facility mainly consists of a stainless steel vacuum tank 0.7 m in diameter and 1.5 m long, a turbo molecular pump system, several DC supplies, and devices explained below. The vacuum tank pressure was kept at about 4×10^{-3} Pa under operations.

PPT

A coaxial PPT with a cavity of a tubular propellant, as shown in Fig.1, was designed for this study. The PPT has an anode inside the tube and a divergent nozzle as a cathode with 20 degrees half-angle at the exit of the cavity. The anode and the cathode are made of tungsten and stainless steel, respectively. The distance between the anode and the cathode is equal to the cavity length. The diameter of the cavity is 3 mm. We designed it smaller than that of conventional electrothermal PPTs in order that the pressure in the cavity rises more highly. The cavity length is variable by varying the position of the anode.

The main discharge was initiated by an igniter mounted in the nozzle. Figure 2 shows the photograph of the firing PPT. Table 1 shows experimental conditions in this study.

Table.1   Experimental conditions.

Stored Energy	E_0	1.06 - 21.4	J
Cavity Length	L	4 - 34	mm
Charging Voltage	V_0	800 - 1800	V
Propellant		Teflon (PTFE)	

Thrust Stand

Impulse bits were measured by a pendulum method, as shown in Fig.3(a). The PPT is mounted on the pendulum. The pendulum rotates around fulcrums of two knife edges without friction. However, three transmission lines for the anode, the cathode and the igniter must be connected to both the pendulum and a flange of the vacuum tank. In order to reduce an undesirable moment by the bending force and weight of lines to the pendulum, these are connected at the rotational axis of the pendulum. The displacement of the pendulum was detected by an eddy-current-type gap sensor (non-contacting micro-displacement meter) near the PPT, which resolution is about ±0.5 μ m. The sensitiveness of pendulum is variable in a range by changing setting positions of the fulcrums and some weights. The sensitiveness was adjusted to 0.70 μ m/μ Ns for lower impulse bit measurements than about 100 μ Ns, and 0.59 μ m/μ Ns for higher impulse bits. The amplitude of the mechanical noise was reduced by an electromagnetic dumper to about ±1 μ m, as shown in Fig.3(b). Thus, errors of the measurement were estimated to about ±2 μ Ns. A typical displacement by firing PPT is shown in Fig.4.

Electromagnetic Dumper   The electromagnetic dumper, as show in Fig.5, was used to suppress mechanical noises and to decrease quickly the amplitude after firing the PPT for the next measurement. It is useful for a sensitive thrust stand because it is non-contacting[4]. The dumper consists of a permanent magnet fixed to the pendulum and two coils fixed to the supporting stand. The control circuit differentiates the output voltage of the displacement sensor and supplies the current proportional to the differentiated voltage to the coil. One coil works if the differentiated voltage is positive, and the other coil works if it is negative. The force is generated in proportion to the coil current. As a result, the dumper works as a viscosity resistor and does not change the balancing position of the pendulum. The dumper was turned off just before firing the PPT for measurements without damping, and turned on after the measurement to prepare for the next measurement.

Calibration   The calibration of impulse was carried out by a collision of a ball to the pendulum[5], as shown in Fig.6. The ball is made of lead and hung by a string with a length of 260 mm and a diameter of
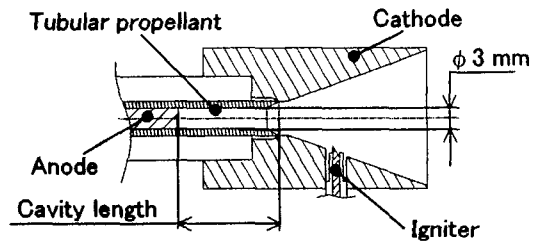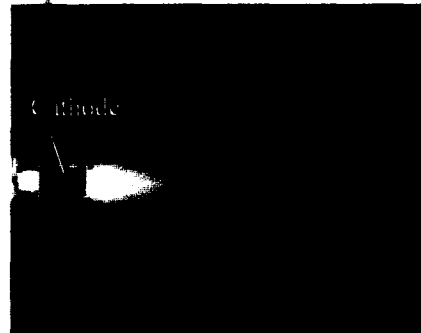

Fig.1 Cross-sectional view of PPT head.

Fig.2   photograph of firing PPT(cavity length: 14mm, stored energy:21.4J).
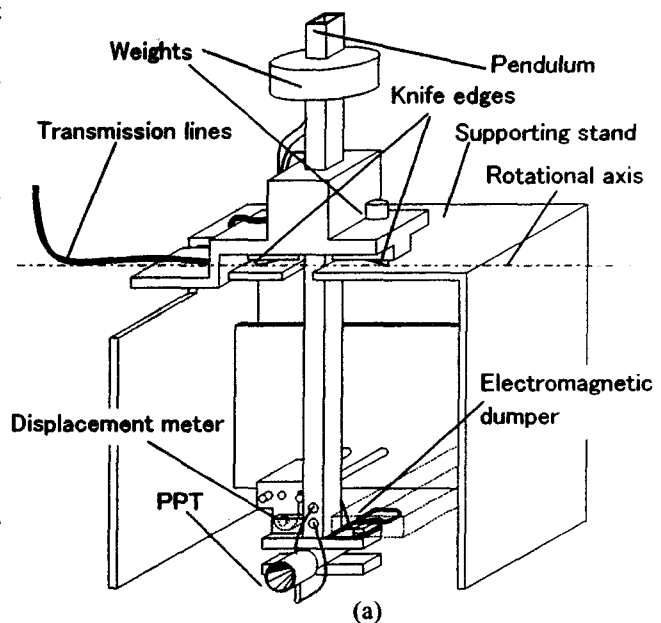

(a)

Fig.3 Thrust stand. (a) Assembly; (b) Mechanical noise before/after dumping.
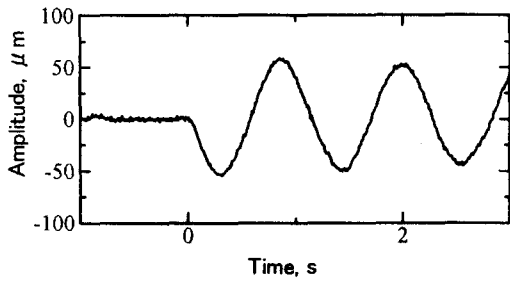
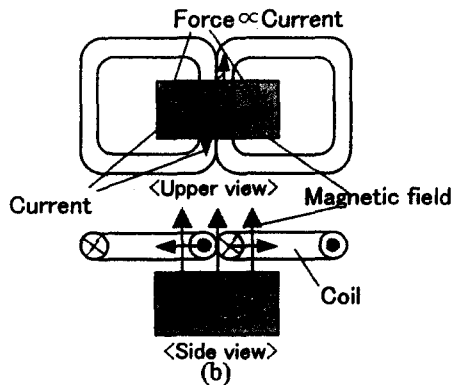Fig.4 Typical response of pendulum by firing PPT.

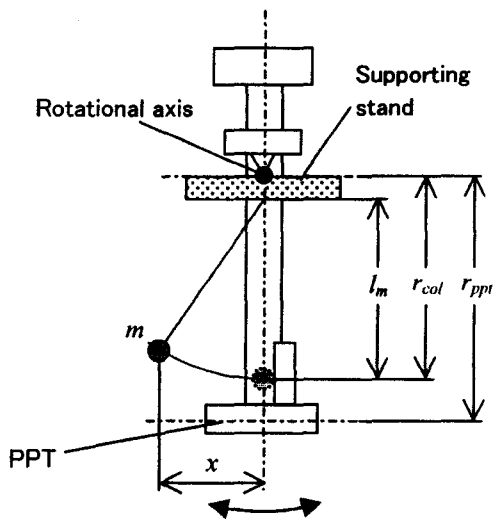Fig.5 Schematic of electromagnetic dumper.
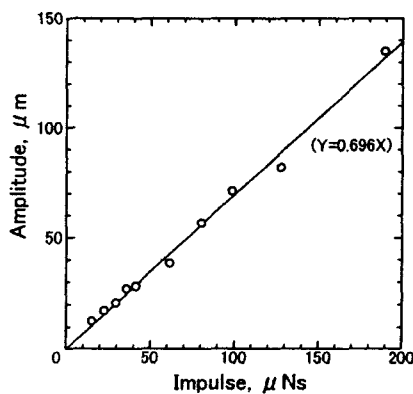

Fig.6 Schematic of calibration.

Fig.7 Typical result of impulse calibration.

0.064 mm. Some balls with different weights of 0.065 - 2.1 g were used for wide-range calibration. An adhesive tape is stuck in the area including the colliding point so that the collision is inelastic. The upper end of the string is connected to the supporting stand at the point near the rotational axis of the pendulum. The difference of balancing positions between before and after colliding is not observed, because the colliding point is arranged on the perpendicular centerline of the pendulum, and the ball is lighter than the pendulum. The impulse for the calibration is calculated as follows.

$$I_{cal} = \frac{m \, r_{col}}{r_{ppt}} \sqrt{2 g l_m \cos\left(\tan^{-1} \frac{x}{l_m}\right)} \qquad (1)$$

where m is the mass of the ball, r_{col} is the distance of the colliding point from the rotational axis, r_{ppt} is the distance of the PPT from the rotational axis, l_m is the distance of the weight from the upper end of the string, and x is the horizontal distance of the ball. Figure 7 shows a typical result of the calibration for lower impulse bit measurements. The calibration was carried out in the atmosphere just before closing the tank. In addition, to guarantee the calibrated value under the low pressure, the triangular pulse current corresponding 80 μ Ns is supplied to one coil of the electromagnetic dumper, and the displacement of the pendulum is measured. This check is carried out once in the atmosphere and several times in the vacuum. The change of the pendulum response is so little that it is negligible.

Measurements of Propellant Mass Loss
A direct-reading balance was used to measure the mass of propellant, which accuracy is 0.1mg. The mass loss per shot was calculated by averaging the total mass loss after 100-300 shots at a frequency of 1 Hz.

Discharge Circuit
Four kinds of capacitances were tested by connecting 1-4 sets of capacitors in parallel. One set has a capacitance of 3.3 μ F, and it consists of three 9.9 μ F capacitors in series. Capacitors are charged to 1.8kV at the maximum in this study. The discharge current waveform is detected by a Rogowski coil.

Results and Discussion

Operational Conditions
The main discharge becomes difficult to occur with increasing cavity length, because the cavity length is equal to the distance between the anode and the cathode. Generation of the main discharge depends on not only the charging voltage but also the stored energy. The main discharges occurred on the conditions satisfied with the following inequality roughly:
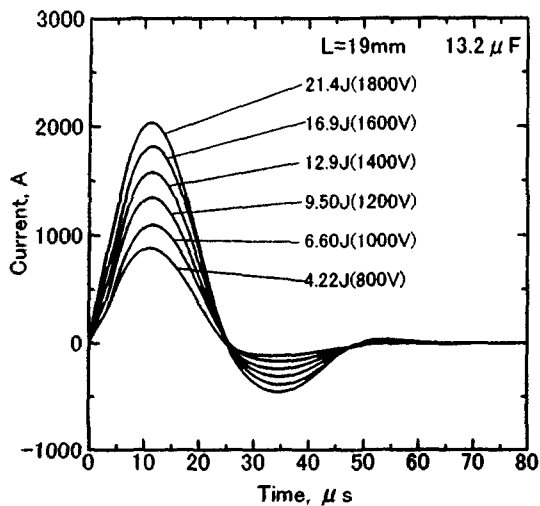
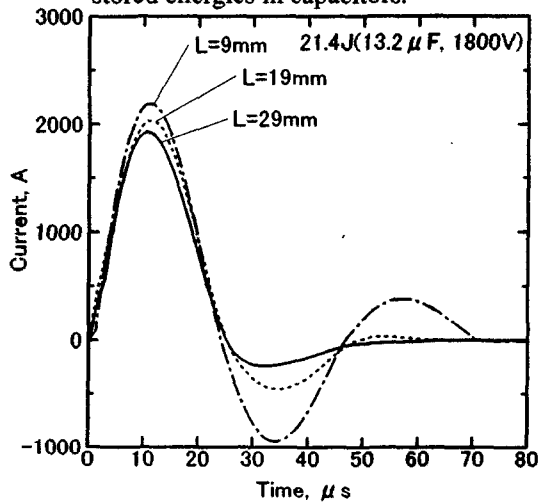Fig.8 Current waveforms for various stored energies in capacitors.

Fig.9 Current waveforms for various cavity lengths.

$$E_0/L \geq 0.12 \, [J/mm] \tag{2}$$

where E_0 is the energy stored in capacitors, and L is the cavity length. The main discharge without the ignition was observed at $L \leq 3$ mm.

Current Waveform

Figures 8 and 9 show current waveforms for different E_0 at a constant cavity length of 19 mm and for different cavity lengths at a constant stored energy E_0 of 21.4 J, respectively. The current peak increases with E_0. Higher current peak is observed for shorter cavity length because the resistance of plasma becomes smaller.

Equivalent Plasma Resistance

In the discharge, the conservation of energy is presented as follows:

$$E_0 = E_{in} + E_{loss} \tag{3}$$

where E_0 is the initially stored energy in capacitors, E_{in} is the energy supplied to the plasma, and E_{loss} is the energy loss in capacitors, transmission lines and electrodes. E_{in} and E_{loss} are written as:

$$E_{in} = \int R_p J^2 dt + \int \frac{L_p}{2} J^2 dt \tag{4}$$

$$E_{loss} = \int (R_{tran} + R_c) J^2 dt \tag{5}$$

where R is the direct-current resistance, and subscrips p , tran and c represent the plasma, the transmission lines including electrodes, and the capacitors, respectively. J is the discharge current. R_c is generally called the equivalent series resistance
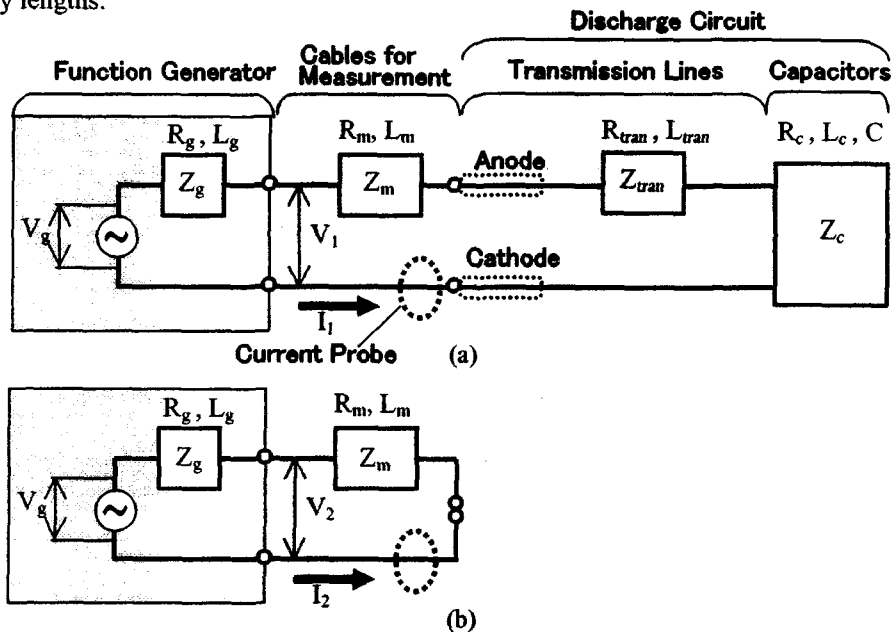

Fig.10 Measurement of circuit parameters by frequency response method.
(a) Including generator, measurement cables, and discharge circuit; (b) Without discharge circuit.

(ESR) of capacitors. In the right side of Eq.(4), the first term is the energy dissipated by joule heating in the plasma, and the second term is the energy used for the electromagnetic acceleration[6]. The equivalent plasma resistance is defined as:

$$R_{p,eq} \equiv \frac{\int (R_p + \dot{L}_p/2) J^2 dt}{\int J^2 dt} \qquad (6)$$

$$= \frac{E_{in}}{\int J^2 dt} \qquad (7)$$

Using Eqs.(3) and (5), E_{in} is written as:

$$E_{in} = E_0 - \int (R_{tran} + R_c) J^2 dt \qquad (8)$$

Assuming that $(R_{tran} + R_c)$ is a constant during the discharge, the transfer efficiency, which is defined as energy into plasma to that stored in capacitors, is as follows:

$$\eta_{tran} \equiv \frac{E_{in}}{E_0} = \frac{1}{1 + \dfrac{R_{tran} + R_c}{R_{p,eq}}} \qquad (9)$$

$R_{p,eq}$, E_{in} and η_{tran} can be calculated from Eqs.(7)-(9) with the current waveform if $(R_{tran} + R_c)$ is acquired.

Parameters of Discharge Circuit

In present study, capacitors exist outside the vacuum chamber, and the total length of transmission lines is approximately 3.5 m × 2 (anode, cathode) = 7m. Thus, the transfer efficiency of the electric circuit is thought low. To estimate parameters of the discharge circuit, frequency responses are measured. Figure 10 shows the schematic of the measurement system. The function generator generates a sinusoidal voltage. The current detected by the current probe and the voltage of the function generator are monitored by a digital oscilloscope. Then the amplitudes of the voltage and the current are recorded with their phase difference. Using the circuit shown in Fig.10(a), the following amount of impedances Z_l is measured:

$$Z_1 \equiv Z_m + Z_{tran} + Z_c = V_1 / I_1 \qquad (10)$$

where Z_m, Z_{tran} and Z_c are impedances of measurement cables, transmission lines including electrodes, and capacitors, respectively. The impedance of measurement cables is measured by connecting each ends of cables, as shown in Fig.10(b):

$$Z_m = V_2 / I_2 \qquad (11)$$

The amplitudes of the function generator signal are fixed at 20 mV, and 10 mV in the measurement in

Figs.10(a) and (b), respectively. From both measurements, $(Z_{tran} + Z_c)$ can be calculated by the subtraction $(Z_1 - Z_m)$. The inductance is calculated assuming a constant capacitance for various angular frequencies:

$$L_{tran} + L_c = \frac{|Z_{tran} + Z_c| \sin \theta + 1/\omega C}{\omega} \qquad (12)$$

where L_{tran} and L_c are inductances of transmission lines including electrodes and capacitors, respectively. θ is the phase difference, and C is the capacitance. L_c is the equivalent series inductance (ESL) of capacitors.

Figure 11 shows measured impedance, resistance and inductance of the discharge circuit for various angular frequencies. Both the resistance and the inductance are roughly constant with the angular frequency. The range of ω in Fig.11 includes all angular frequencies of discharge current waveforms in this study. Table 2 shows $(R_{tran} + R_c)$ and $(L_{tran} + L_c)$ at the minimum impedance. The resistance do not show clear tendency on the difference in capacitances although the inductance has a clear tendency to decrease with increasing capacitance. Therefore, it is suggested that most of the resistance is due to that of the transmission lines, and that the difference of resistances in Table 2 is thought as the measurement error.
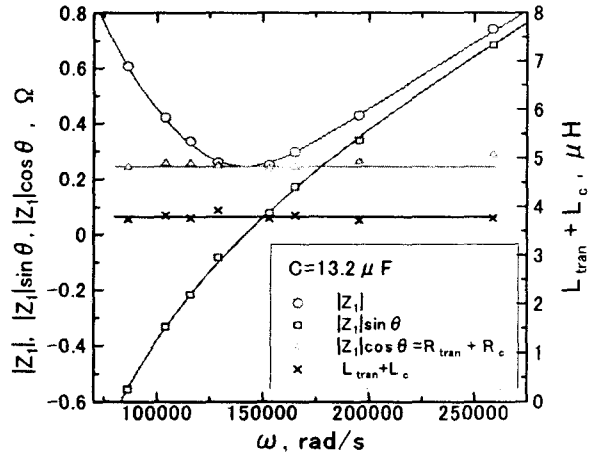

Fig.11 Dependence of circuit parameters on angular frequency.

Table 2   Parameters of discharge circuit.

Capacitance μF	$R_{tran} + R_c$ Ω	$L_{tran} + L_c$ μH
3.3	0.252	4.19
6.6	0.231	3.98
9.9	0.253	3.80
13.2	0.241	3.76
Average	0.244	3.93

E_{in} is calculated from Eq.(8) with the average value of $(R_{tran} + R_c)$ and the current waveform. Figure

12 shows E_{in} plotted versus the integration of J^2 for various capacitances and charging voltages at a cavity length of 19 mm. In this figure, different plots with the same capacitance have different charging voltages. The slope means the equivalent plasma resistance defined in Eq.(7). The $R_{p,eq}$ is roughly proportional to the integration of J^2. Thus $R_{p,eq}$ is not dependent on the charging voltage nor the capacitance. The $R_{p,eq}$ was calculated by the least square method for various cavity length and plotted in Fig.13 as a function of the cavity length. The $R_{p,eq}$ increases in proportion to the cavity length, so that $R_{p,eq}$ is fitted as:

$$R_{p,eq}[\Omega] \approx 0.01094 \times L[mm] \qquad (13)$$

thus, the transfer efficiency becomes as follows:

$$\eta_{tran} \approx \frac{1}{1 + 22.3 / L[mm]} \qquad (14)$$

η_{tran} and the energy density E_{in}/V [J/mm^3] is plotted in Fig.14, where V is the cavity volume.
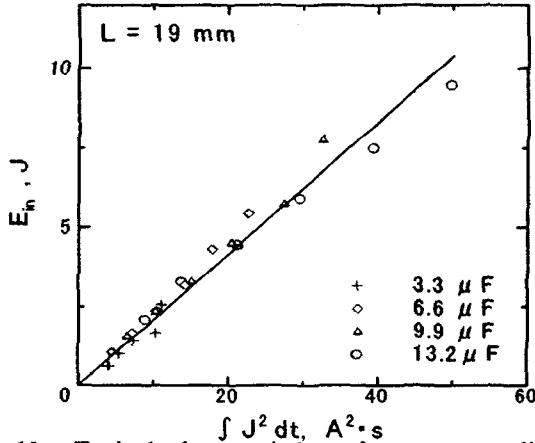

Fig.12 Typical characteristics of energy supplied to plasma vs integration of the square of discharge current.
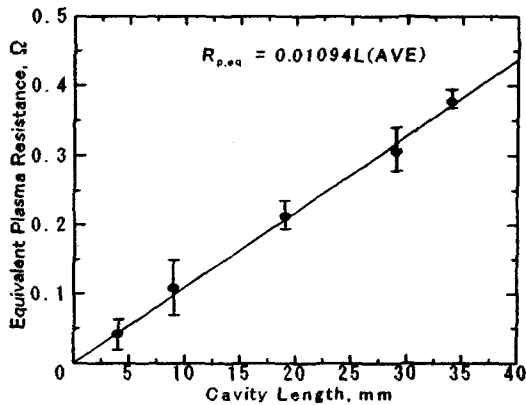

Fig.13 Equivalent plasma resistance vs cavity length.

Impulse bit

Figures 15(a) and (b) show the impulse bit versus E_0 and E_{in}, respectively. Impulse bit linearly increases
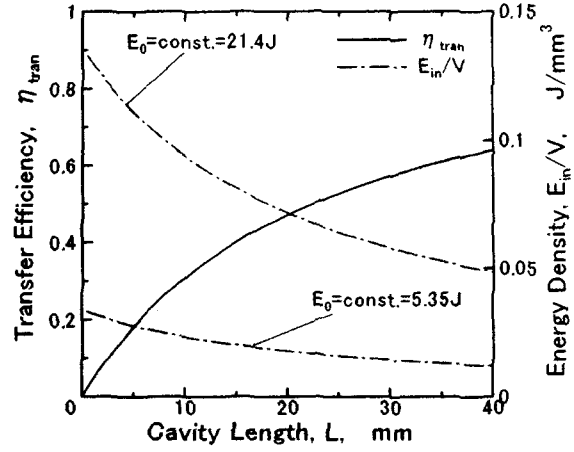

Fig.14 Transfer efficiency and energy density vs cavity length.

with E_0 and E_{in}. But the difference by the cavity length in Fig 15(b) is smaller than that in Fig.15(a). Then, the impulse bit I_{bit} is fitted using E_{in}:

$$I_{bit} \approx 87.9 E_{in} - 33.7 \quad [\mu Ns] \qquad (15)$$

Figures 16(a) and (b) show the impulse bit per unit E_0 and unit E_{in}, respectively. They are low at low E_0 and E_{in}, and roughly constant for high E_0 and E_{in}. It is because fitting lines in both Fig.15(a) and (b) cross with x-axis at positive values.

Propellant Loss

Figures 17(a) and (b) show the propellant loss per unit E_0 and unit E_{in}, respectively. They are roughly constant with E_0 and E_{in}, respectively. Then, the least square method was used for the plot of both Δm vs E_0 and Δm vs E_{in}. Both $\Delta m/E_0$ and $\Delta m/E_{in}$ were plotted versus L in Fig.18. They linearly increase with the cavity length, and $\Delta m/E_{in}$ is fitted as:

$$\Delta m / E_{in}[\mu g / J] = 0.425(L[mm] + 18.1) \qquad (16)$$

This tendency is because of higher energy density for shorter cavity length, as shown in Fig.14. Eq.(16) can be written as follows using Eqs.(14),:

$$\Delta m / E_0 = 0.425 f(L)L \qquad (17)$$

here,

$$f(L) \equiv (L + 18.1)/(L + 22.3) \qquad (18)$$

Within the operational condition, $f(L)$ is from 0.84 to 0.92. Therefore $f(L)$ can be regarded as a constant roughly, and then $\Delta m/E_0$ seems to be proportional to L. However, as η_{tran} approaches unity, the curve of $\Delta m/E_0$ versus L will approach the line of Eq.(16). For example, some curves of Eq.(17) were drawn for various $(R_{tran} + R_c)$ in Fig.18. Then it will not be regarded as proportional to L. For instance, we can see Figure 7 in Ref.2) as a part of this tendency.
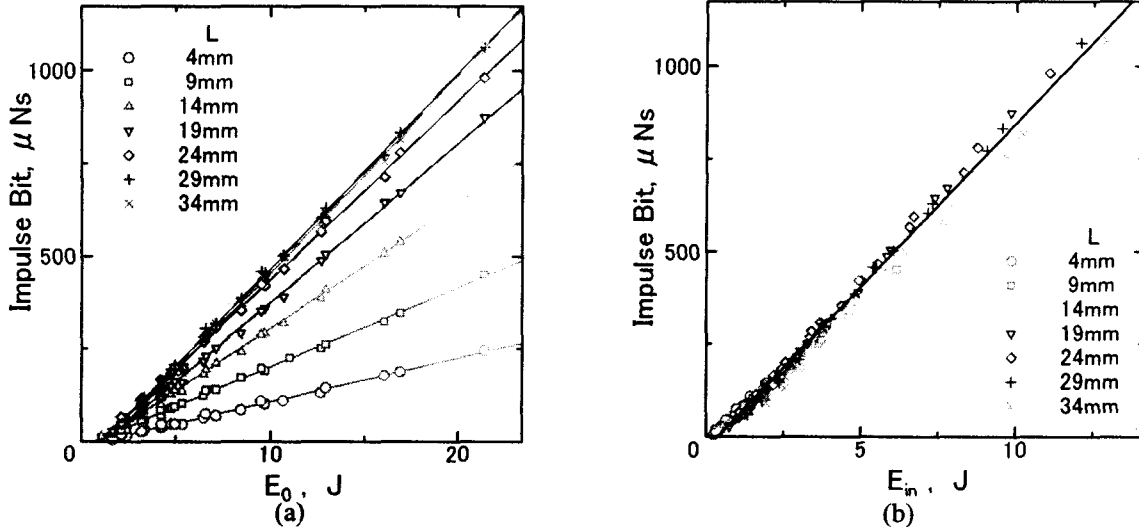
Fig.15 Impulse bit vs E_0 and E_{in}. (a) Arranged by E_0 ; (b) Arranged by E_{in}.
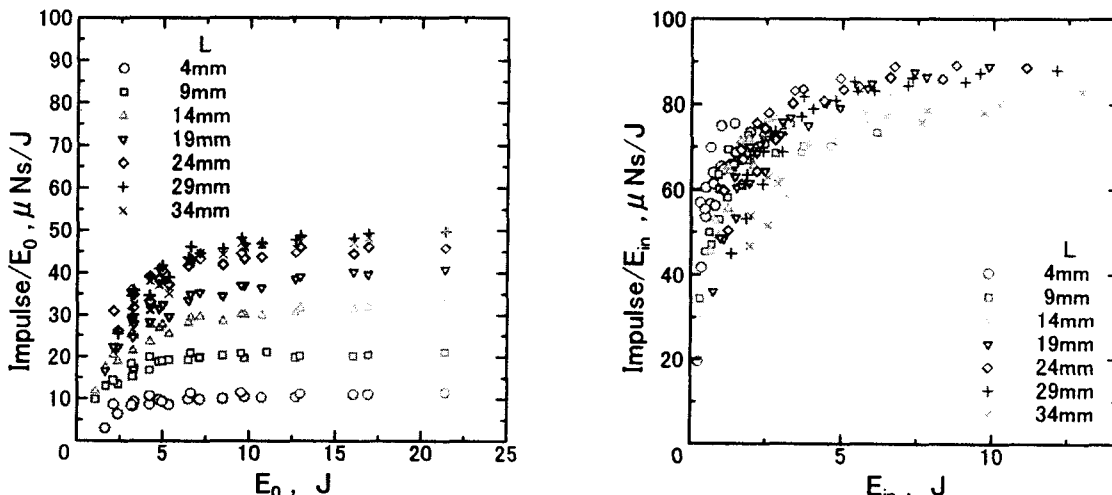(E_0: energy stored in capacitors, E_{in}: energy supplied to plasma)

Fig.16 Impulse bit per unit E_0 vs E_0, and impulse bit per unit E_{in} vs E_{in} .(a) Arranged by E_0;
(b) Arranged by E_{in}. (E_0: energy stored in capacitors, E_{in}: energy supplied to plasma)
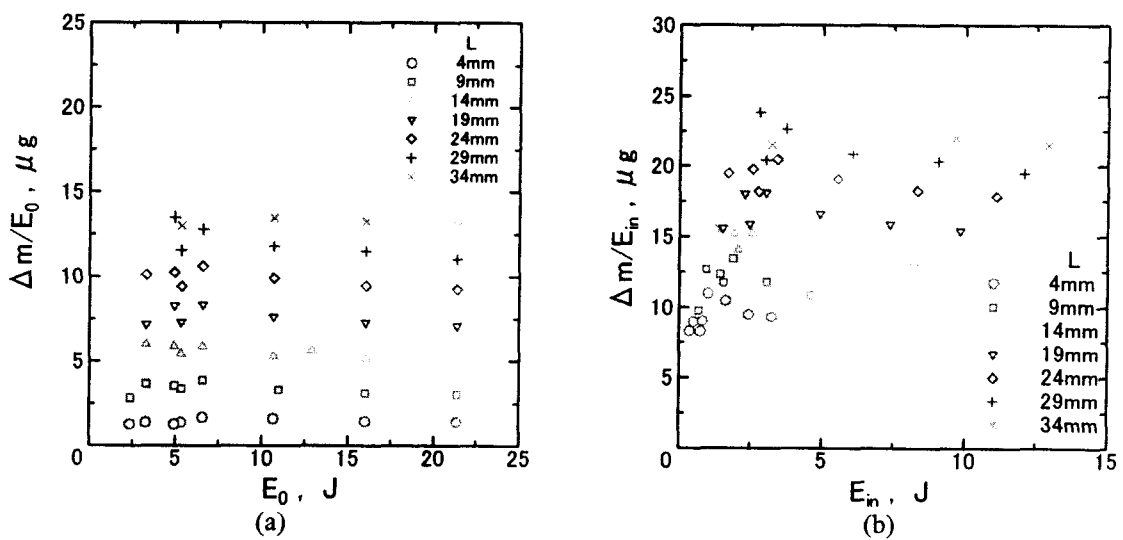

Fig.17 Propellant mass loss per unit E_0 vs E_0, and propellant mass loss per uinit E_{in} vs E_{in}.
(a) Arranged by E_0; (b) Arranged by E_{in}. (E_0: energy stored in capacitors, E_{in}: energy supplied to plasma)
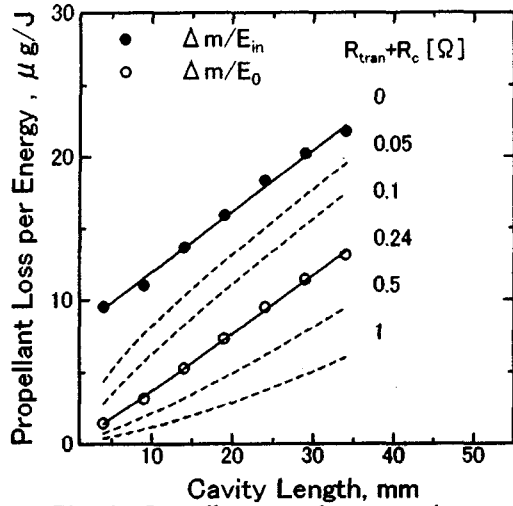
Fig.18 Propellant mass loss per unit energy vs cavity length.

Specific Impulse

Figures 19 (a) and (b) show the specific impulse versus E_0 and E_{in}, respectively, for various cavity length. Higher specific impulse is obtained for shorter cavity length and for higher E_{in}, because of higher energy density, as shown in Fig.14. Assuming the ideal gas heated in a constant cavity volume, the pressure in the cavity is written as:

$$P = (\gamma - 1)E_{in}/V \qquad (19)$$

where P is the pressure in the cavity, γ is the ratio of the specific heats, and V is the cavity volume. Then, E_{in}/V represents the energy density. However, in actual, plasma gas, which has leaked out of the cavity, exists in the nozzle when the cavity pressure is at maximum[7], so that the pressure is not as high as that of Eq.(19). But the plasma in the nozzle is accelerated by the electromagnetic force induced by

the divergent current. As shown in Fig.9, the current peak is higher for shorter cavity length. Consequently, the accelerating force is higher at shorter cavity length, though the fraction of the electromagnetic acceleration is unknown.

Energy Efficiencies

Burton, R.L., et al defined various energy efficiencies in Ref. 2). In this paper, we considered the following efficiencies, the thrust efficiency η_t, the transfer efficiency η_{tran}, and the acceleration efficiency η_{acc}.

$$\eta_t = E_t / E_0 \qquad (20)$$

$$\eta_{tran} = E_{in} / E_0 \qquad (21)$$

$$\eta_{acc} = E_t / E_{in} \qquad (22)$$

where E_t is the thrust energy. We measured η_t and η_{tran}, and estimated η_{acc} by following equation:

$$\eta_t = \eta_{tran} \times \eta_{acc} \qquad (23)$$

The thrust efficiency η_t measured, the transfer efficiency η_{tran} decided by Eq.(14), and the acceleration efficiency η_{acc} calculated from η_t (fitting curve was used) by Eq.(23) are shown in Fig.20. They are plotted versus the cavity length. η_t shows a low peak or saturation around the cavity length of 15-30 mm. η_{tran} increases with the cavity length, approaching $\eta_{tran} = 1$. η_{acc} is higher for shorter cavity length, because of higher energy density E_{in}/V. In other words, η_t falls mainly by the transmission loss if the cavity length is short, and η_t falls mainly by the acceleration loss if the cavity length is long. As a result, η_t has a low peak or saturation region, and it is thought that the
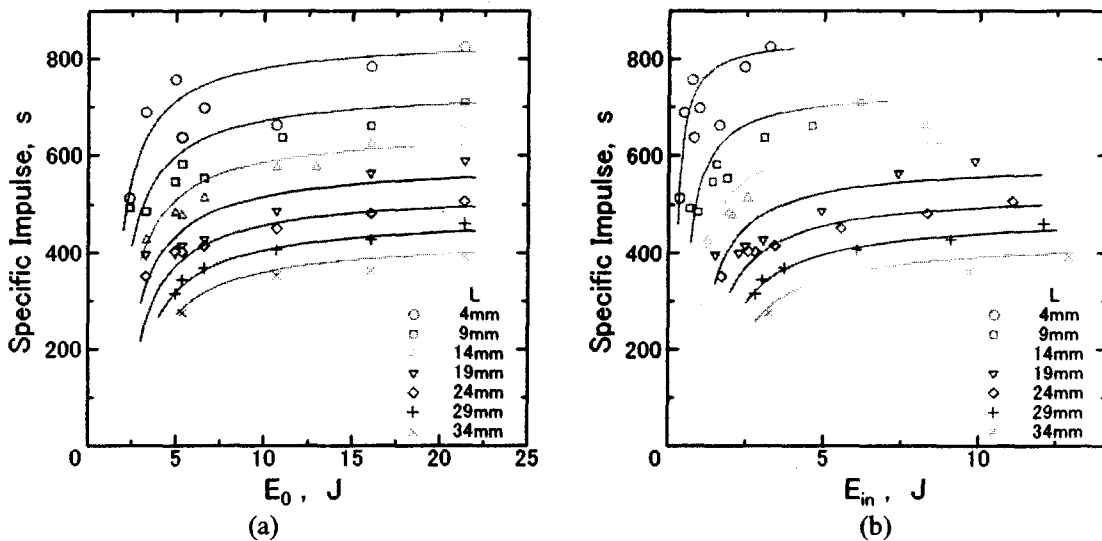

(a)

(b)

Fig.19 Specific impulse vs E_0 and E_{in}. (a) Arranged by E_0 ; (b) Arranged by E_{in}. (E_0: energy stored in capacitors, E_{in}: energy supplied to plasma)

optimal cavity length becomes shorter if η_{tran} is improved. In this figure, E_{in} is not constant with the cavity length, because η_{tran} varies with the cavity length. η_{acc} versus E_{in} was shown in Fig.21, excluding the influence of η_{tran}. Each curve was drawn using the fitting curve mentioned below, within the operational condition. This figure shows the stronger tendency of high η_{acc} for short cavity length.

Fitting Curves for Energy Efficiencies

The fitting curve of the thrust efficiency can be derived by Eqs.(15) and (17), but it did not fit to the result well. It is because of the fitting error of each equation. Then, it was attempted to derive the fitting curve by comparison of E_t and E_{in}. Figure 22 shows E_t versus E_{in} for various cavity length. E_t linearly increases with E_{in}, as:

$$E_t = A(L)\{ E_{in} - B(L) \} \qquad (24)$$

where A and B are constants depending on the cavity length. A and B were calculated by the least square method, and plotted in Fig.23. And A and B were fitted as follows by the least square method:

$$A(L) = 0.337 - 0.00411L \qquad (25)$$
$$B(L) = 0.0528\ L \qquad (26)$$

Then, the thrust efficiency is derived from Eqs.(24)-(26):

$$\eta_t = A(L)\{E_{in} - B(L)\}/E_0 \qquad (27)$$
$$= A(L)\{\eta_{tran}(L) - B(L)/E_0\} \qquad (28)$$

Fitting curves for other parameters can be derived from their definition with Eqs. (16)-(18) and (25)-(28).
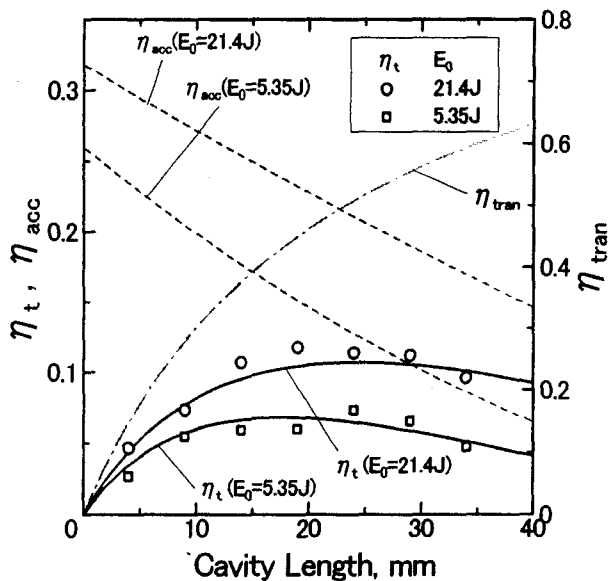

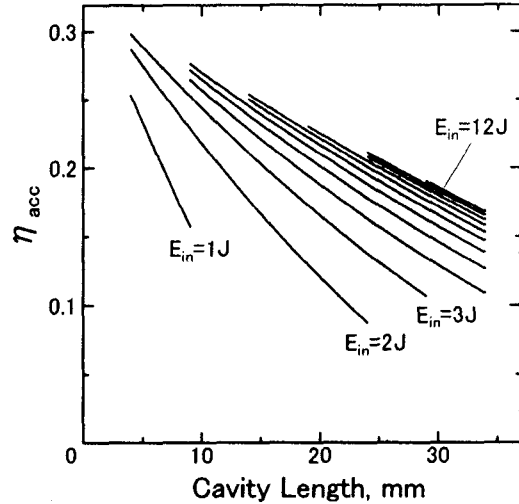Fig.21　Acceleration efficiency vs cavity length.
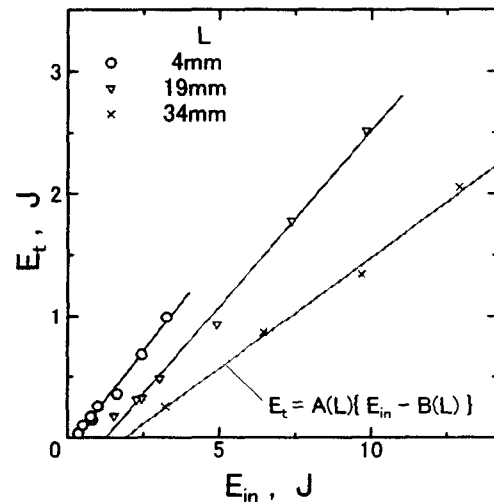
Fig.22　Thrust energy vs energy supplied to plasma.
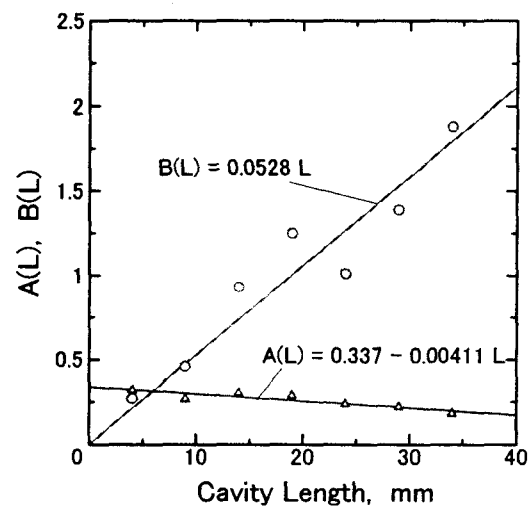

Fig.20　Energy efficiencies vs cavity length.

Fig.23　Dependence of parameters in acceleration efficiency on cavity length.

Impulse Bit per Unit Stored Energy vs Specific Impulse

Figure 24 shows the impulse bit per unit E_0 versus the specific impulse. It is showed that the performance of this PPT approached that of electromagnetic PPT with decreasing cavity length because of the reason suggested in the paragraph of Specific Impulse. Using Eqs.(17) and (18), the impulse bit per unit E_0 is written as follows:

$$I_{bit} / E_0 = \{0.425\, g\, f(L) L\} I_{sp} \qquad (29)$$

where I_{sp} is the specific impulse. This equation shows that the impulse bit per unit E_0 is proportional to the specific impulse at a fixed cavity length. Dash lines were drawn by Eq.(29).
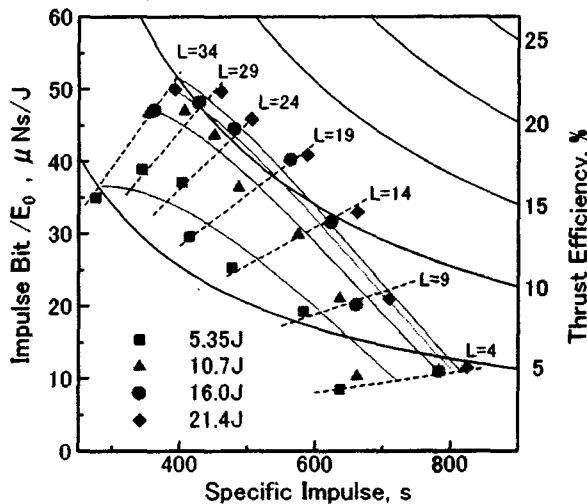

Fig.24　Impulse bit per unit stored energy vs specific impulse.

Changes in Performances during Shots

Impulse bit and propellant loss changed slowly during repetitive shot, shown in Fig.25. This is because the cavity diameter increased during shots. The error in the propellant loss measurement by the change during shots is negligible, because the propellant loss was estimated during the first 300 shots at most. But the change of the impulse bit was not negligible within 300 shots, so the impulse bit was measured within the first 100 shots. Therefore, all data in this paper should be considered as the initial performances.

Conclusions

The coaxial pulsed plasma thruster with the Teflon cavity was designed, and its performance characteristics were examined. Following results were obtained.

(1) The resistance and the inductance of the discharge circuit were roughly constant with varying oscillation frequency.
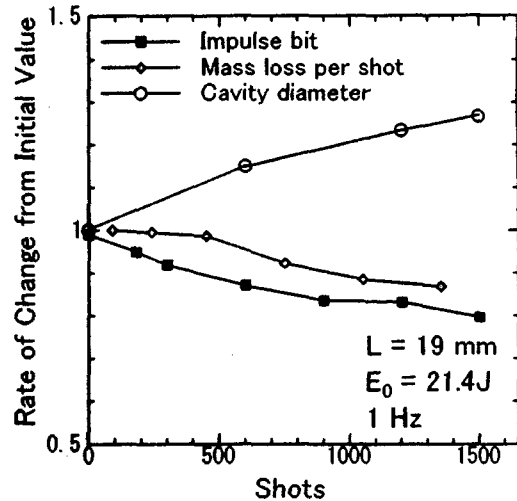

Fig.25　Changes of impulse bit, mass loss and cavity diameter during repetitive shots at 1Hz.

(2) The equivalent plasma resistance, which determines the energy supplied to the plasma, was defined, considering the energy conservation during the discharge. It increased in proportion to the cavity length. Therefore, the current peak decreased with increasing cavity length. The proportional constant was 0.01094 Ω/mm, corresponding the resistivity of 7.7×10^{-5} Ωm.

(3) Using the circuit resistance and the equivalent plasma resistance, the transfer efficiency was determined as a function of the cavity length.

(4) Impulse bit linearly increased with the energy stored in capacitors. The difference of the impulse bit by the cavity length became smaller if it was plotted as a function of the energy supplied to the plasma.

(5) The propellant loss was proportional to the energy supplied to the plasma. It increased with the cavity length linearly, but it was not proportional, because the energy density was larger for shorter cavity length.

(6) Both the specific impulse and the acceleration efficiency increased with decreasing cavity length or increasing energy supplied to the plasma, because both the energy density and the current peak increased.

(7) As a whole system, as the cavity length became shorter, the thrust efficiency fell by the transmission loss mainly. As the cavity length became longer, it fell by the acceleration loss mainly. Consequently, there was the optimal cavity length for the thrust efficiency.

(8) The performance of this PPT approached that of electromagnetic PPT with decreasing cavity length.

(9) This PPT achieved thrust efficiencies of 10-12% at 21.4 J and 6-7% at 5.35 J at cavity lengths between 14 mm and 29 mm, and those are not low performances in comparison with other typical PPTs with near-energies. Higher performance can be

expected by locating capacitors near the PPT.

References

1) Burton, R. L., and Turchi, P. J., "Pulsed Plasma Thruster," Journal of Propulsion and Power, Vol. 14, No. 3, Sep.-Oct., 1998, pp. 716-735.

2) Rysanek, F., and Burton, R. L., "Performance and Heat Loss of a Coaxial Teflon Pulsed Thruster," 27th International Electric Propulsion Conference, Pasadena, CA, USA, Paper IEPC-01-151, 2001.

3) Burton, R. L., Wilson, M. J., and Bushman, S. S., "Energy Balance and Efficiency of the Pulsed Plasma Thruster," AIAA Paper No.98-3808, July, 1988.

4) Koizumi, H., Kakami, A., Furuta, Y., Komurasaki, K., and Arakawa, Y., "Liquid Propellant Pulsed Plasma Thruster," 28th International Electric Propulsion Conference, Toulouse, France, Paper IEPC-03-087, 2003.

5) Kameoka, M., Takegahara, H., Shimizu, Y., and Toki, K., "Single Pulse Measurement of a Coaxial Pulsed Plasma Thruster," 28th International Electric Propulsion Conference, Toulouse, France, Paper IEPC-03-093, 2003.

6) 栗木恭一, 荒川義博編 "Introduction to Electric Propulsion 電機推進ロケット入門," 東京大学出版会, 第 8 章, 2003, pp.157-181.

7) Keider, M., Boyd, I. D., and Beilis, I. I., "Model of an Electrothermal Pulsed Plasma Thruster," Journal of Propulsion and Power, Vol. 19, No. 3, May-June 2003, pp. 424-430.